Analysis of Movable Louvers for Temperature Control

JOSEPH A. PLAMONDON*
Jet Propulsion Laboratory, California Institute of Technology, Pasadena, Calif.

Movable shutters or louvers are being employed on several spacecraft for active thermal control. The present analysis of an infinite louver array led to seven equations; six of them form a simultaneous set (three linear integral equations and three linear algebraic equations) which describes the heat-transfer characteristics of the array, and the seventh gives its relative thermal performance in terms of an effective emissivity. The equations are solved numerically, and effective emissivity is plotted as a function of louver blade position for various values of the dimensionless parameters that appear in the governing heat-transfer equations. The results are compared with experimental results obtained for the Mariner II spacecraft louver system; agreement is good when the test data are corrected for power dissipation from auxiliary hardware and the end losses of the finite array. The remaining 4.5% discrepancy at the full-open position is attributed to specular (rather than the assumed diffuse) reflection from the blades.

Nomenclature

b	=	blade width, ft
B, C, D	=	local radiosity at x, y, and z, respectively, Btu/ft²-hr
B^*, C^*, D^*	=	local dimensionless radiosity at β, ζ, and η, respectively; $B(\beta)\sigma T_1^4$, $C(\zeta)/\sigma T_1^4$, and $D(\eta)/\sigma T_1^4$
dF_{i-j}	=	incremental view factor, from di to dj, where $i = x, y, z$; $j = x, y, z$; $i \neq j$
H	=	local irradiance, Btu/ft²-hr
K	=	see Eqs. (11–13)
L	=	blade spacing, ft
M	=	view-factor from incremental area $d\beta$, $d\zeta$, or $d\eta$ to open end of channel
$q''(x)$	=	local heat-transfer rate from back surface, Btu/ft²-hr
$q''^*(x)$	=	dimensionless local heat-transfer rate from back surface, $q''(\beta)/\sigma T_1^4$
T	=	local temperature, °R
T^*	=	local dimensionless temperature T^4; e.g., at ζ, $\sigma T_2^4(\zeta)/\sigma T_1^4$
x	=	coordinate along back surface, ft
y, z	=	coordinates along inside and outside of blades, ft
α	=	absorptivity
γ	=	$1 - \cos^2\theta$, definition
ρ	=	reflectivity
ϵ	=	graybody hemispherical emissivity
β, ζ, η	=	dimensionless coordinates, x/L, y/L, z/L
θ	=	blade opening angle
σ	=	Stefan-Boltzmann constant

Subscripts

1	=	back surface
2	=	inside blade surface
3	=	outside blade surface
T	=	effective value for total array

Introduction

THERMAL management or temperature control of a spacecraft is accomplished by creating a balance, within prescribed temperature tolerances, between the rates of heat absorption and heat rejection. For many spacecraft, this balance is obtained by passive means, that is, the absorptivities of surfaces exposed to external heat sources and the emissivities of surfaces rejecting heat to space are selected to provide a balance of total heat input and output at acceptable temperatures. However, as spacecraft become larger and more complex, active and positive control over the thermal parameters will be required.

Many schemes have been proposed, but few have been developed and flight-tested. One active system, which was used successfully on the Mariner II Venus flyby, consists of an array of low-emissivity, movable blades, whose movement is controlled by bimetallic sensors set for a predetermined temperature range. This array is placed over a surface of relatively high emissivity. When the array is closed, it acts as a single radiation shield against the dissipation of heat from the high-emissivity surface to space; as the blades open, the radiative view factor to space for the high-emissivity surface increases, thus controlling the rate of radiative heat rejection.

Because louver systems have been successfully flown and will undoubtedly be flown again, an analysis was undertaken to better understand the basic parameters that influence their thermal behavior. This paper presents the formulation and results of the analysis.

Assumptions

The assumptions made in the analysis are, in part, incorporated in the mathematical model shown in Fig. 1. The coordinate axis x lies along the back surface, y lies along the inside of the louver blades, and z lies along the outside of the louver blades. The louver blade opening angle is θ (zero for the closed position). The most significant simplifications result from the following assumptions: 1) The array is infinite in width and the blades are infinite in length (into paper); 2) all blades have the same θ; 3) the gap distance between the array and the back surface approaches zero;

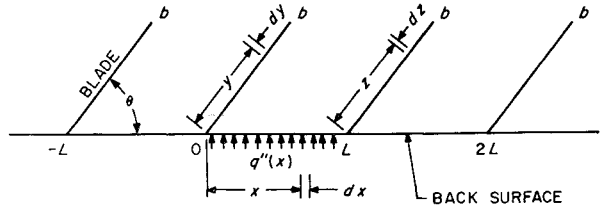

Fig. 1 Mathematical model of louver array.

Received January 13, 1964; revision received April 1, 1964. This paper presents the results of one phase of research carried out at the Jet Propulsion Laboratory, California Institute of Technology, under Contract No. NAS 7-100, sponsored by NASA. We are grateful to Marshall Gram, of JPL, who kindly supplied the experimental data collected on the Mariner II system, and also to Ted Cullen, who programed the equations for the numerical solution.

* Research Engineer. Member AIAA.

4) conduction in the blades in the y or z direction is negligible; 5) no temperature drop exists through the blades (normal to the y or z direction); 6) emissivities of the inside and outside blade surfaces are equal ($\epsilon_2 \equiv \epsilon_3$); 7) temperature of the back surface is uniform; and 8) the blades and the back surface emit and reflect diffusively.

The first three assumptions are made out of necessity, since without them analysis would be formidable. The first and second assumptions force the thermal events within each channel, formed by two successive louver blades, to be identical by eliminating end-effects and by making the configuration of each channel identical. The third assumption restricts interreflections between the back surface and the blades to one channel, since that portion of the back surface, between two successive blades, can see only the two blades. These three assumptions, therefore, reduce the analysis to a consideration of only one channel. The first assumption is fairly reasonable, because an array usually is made up of quite a few blades, and a guard or sealing ring is placed around the array. The second assumption is reasonable if 1) all blades are actuated by a single actuator, or 2) adjacent actuators for individually actuated blades sense nearly the same actuating input. The third assumption somewhat distorts local heat-transfer characteristics; however, the assumption has no effect on the over-all thermal characteristics of an array because in an infinite array the amount of energy escaping through the louvers is independent of the blades' pivotal position relative to the back surface.

The fourth assumption reduces the resulting set of integro-differential equations to linear integral equations, since it eliminates conduction from the analysis. This assumption, along with assumption 5, is reasonable for the basis of the Mariner II louver design, for which the blades were only 0.005 in. thick. Assumption 5 is reviewed in the final section of this paper. The sixth assumption results from current louver design practice. Assumptions 5 and 6 simplify the heat balance equation in the blades. The seventh assumption may also be valid, because the surface to which a louver array is mounted will usually serve also as a mounting surface for electronic components; hence it will be thick enough to produce reasonably uniform temperatures.

Of the eight assumptions, the eighth is the most compromising and least valid. In the design of a louver system, the emissivity of the back surface is made as high as possible to give maximum control over heat dissipation through the array. It is also desirable to make the louver blades of a material that reflects energy specularly, which is, generally, the reflectance characteristic of low-emissivity surfaces, especially when the energy spectrum is primarily in the infrared region. In the fully open position, specularly reflecting blades tend to minimize the amount of energy that returns to the back surface after an interaction with the blades, but the advantageous effect of specularity decreases as the blades close. However, to have made the analysis on the basis of specular rather than diffuse blade surfaces would have so complicated the governing integral equations that a solution would not have been feasible at this time.

Along with the forementioned eight assumptions, these generally accepted assumptions are listed: heat transfer to space is solely by radiation; space is effectively at 0°R; all surfaces are gray reflectors and emitters; all material properties are constant; and no external sources of energy exist.

Mathematical Formulation

In deriving the heat-transfer equations, the so-called radiosity approach[1] is used. From Fig. 1 it is obvious that symmetry does not exist, and, therefore, it is necessary to write a separate radiosity equation for each surface making up the channel. The differentials dx, dy, and dz represent differential areas on the back surface, inside blade surface, and outside blade surface, respectively. For convenience, the back surface is denoted by 1, the inside blade surface by 2, and the outside blade surface by 3. For each differential area, radiant flux (emitted energy plus reflected energy) leaving points x on 1, y on 2, and z on 3 are denoted by B, C, and D, respectively. The emitted energy is given by the Stefan-Boltzmann law. The irradiance (incident energy) on dx, dy, and dz denoted by H_1, H_2, and H_3, respectively, is expressed so that the reflected energy flux is given by $\rho H(\text{arg}) = (1 - \alpha)H(\text{arg})$, where α is the absorptivity. For gray-bodies, $\alpha = \epsilon$. With these definitions, the radiosity equation for the point x on surface 1 can be written

$$B = \epsilon_1 \sigma T_1^4 + \rho_1 H_1 \tag{1}$$

and similar expressions apply for C and D onto surfaces 2 and 3, respectively. The temperature T_1 is constant because of assumption 6.

Since all surfaces are planar and cannot see themselves, and since no external sources of radiant energy exist, the irradiance on dx at x is composed of that portion of the flux leaving all points on 2 and all points on 3 and arriving at dx. (Similarly, the irradiance on dy at y is composed of the flux leaving surfaces 1 and 3 and arriving at dy, and likewise, for dx on z.) Then CdF_{y-x} is the flux leaving dy incident on dx when dF_{y-x} is the geometrical view-factor of dx as seen from dy, where, by reciprocity, $dF_{y-x}dy = dF_{x-y}dx$. Total flux incident on dx from surface 2 is, therefore, given by $\int_0^b C dF_{x-y}$. Applying the same reasoning to obtain the total flux incident on dx at x from surface 3, and for the incident fluxes on dy and dz from the appropriate surfaces, one obtains

$$H_1 = \int_0^b C\, dF_{x-y} + \int_0^b D\, dF_{x-z} \tag{2}$$

$$H_2 = \int_0^L B\, dF_{y-x} + \int_0^b D\, dF_{y-z} \tag{3}$$

$$H_3 = \int_0^L B\, dF_{z-x} + \int_0^b C\, dF_{z-y} \tag{4}$$

The two-dimensional incremental geometric view-factor is given[2] by the simple expression $dF_{i-j} = \frac{1}{2}d(\sin\phi)$, where ϕ is the angle formed by the outward normal from i and the radius vector from i to j. The expressions for the differential geometric view-factors are

$$dF_{x-y}dx = dF_{y-x}dy = K_{x-y}dxdy \tag{5}$$

$$dF_{x-z}dx = dF_{z-x}dz = K_{x-z}dxdz \tag{6}$$

$$dF_{y-z}dy = dF_{z-y}dz = K_{y-z}dydz \tag{7}$$

Substituting Eqs. (2–7) into Eq. (1) and the analogous equations for C and D gives

$$B = \epsilon_1 \sigma T_1^4 + (1 - \epsilon_1)\left(\int_0^b CK_{x-y}dy + \int_0^b DK_{x-y}dz\right) \tag{8}$$

$$C = \epsilon_2 \sigma T_2^4(z) + (1 - \epsilon_2)\left(\int_0^L BK_{x-y}dx + \int_0^b DK_{y-z}dz\right) \tag{9}$$

$$D = \epsilon_2 \sigma T_3^4(z) + (1 - \epsilon_2)\left(\int_0^L BK_{x-z}dx + \int_0^b CK_{y-z}dy\right) \tag{10}$$

where

$$K_{x-y} \equiv \tfrac{1}{2}\gamma xy(x^2 + y^2 - 2xy\cos\theta)^{-3/2} \tag{11}$$

$$K_{x-z} \equiv \tfrac{1}{2}\gamma z(L - x)[(L - x)^2 + z^2 + 2z(L - x)\cos\theta]^{-3/2} \tag{12}$$

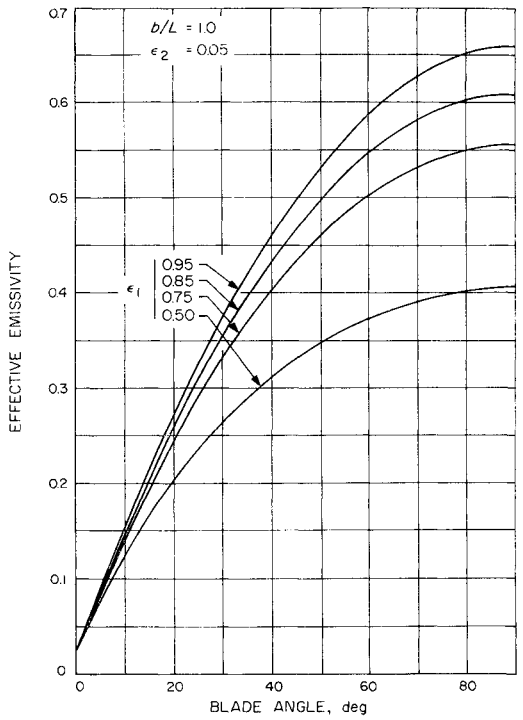

Fig. 2 Effective emissivity vs blade opening angle for various values of ϵ_1.

$$K_{y-z} \equiv \tfrac{1}{2}\gamma L^2[(z-y)^2 + L^2 + 2(z-y)L\cos\theta]^{-3/2} \quad (13)$$

$$\gamma \equiv 1 - \cos^2\theta \quad (14)$$

Next, the net energy flux dissipated at x from the back surface is denoted by $q''(x)$, where $q''(x)$ is the internal heat-generation rate at x. This is related to the total energy dissipation rate at x by the expression

$$q''(x) = \epsilon_1\sigma T_1^4 - \alpha_1 H_1 = \epsilon_1[\sigma T_1^4 - H_1] \quad (15)$$

where $\epsilon_1 \equiv \alpha_1$. Solving for H_1 in Eq. (1) and substituting into Eq. (15) gives

$$q''(x) = \epsilon_1(\sigma T_1^4 - B)/(1-\epsilon_1) \quad (16)$$

Since energy is not generated internally in the louver blades, the equivalent of Eq. (15) for the location y or z on the blade is

$$\epsilon_2\sigma T_2^4 + \epsilon_2\sigma T_3^4 = \alpha_2 H_2 + \alpha_2 H_3 \quad (17)$$

when $y = z$, and from assumption 5, $T_2 = T_3$ when $y = z$; hence

$$2T_2^4 = 2T_3^4 = C + D \quad (18)$$

when $y = z$. Investigation of Eqs. (8–10, 16, and 18) shows that the mathematical formulation of heat transfer through an array of louver blades from the back surface produces a set of six equations (three of which are integral equations) with six unknowns, namely, B, C, D, $q''(x)$, T_2 and T_3.

Now, let the effective emissivity of the array be defined as the ratio of net heat transfer from the back surface to that amount of heat that would be dissipated if the back surface were a fully exposed blackbody, so that

$$\epsilon_T L\sigma_1 T_1^4 = \int_0^L q''(x)dx \quad (19)$$

This definition is independent of actuation techniques so long as the back-surface temperature gradient is small between successive channels.

In order to write the foregoing equations in dimensionless form, the substitutions $x = \beta L$, $y = \zeta L$, and $z = \eta L$ were made, and then all equations were divided by σT_1^4. Thus, B is transformed to B^*, etc., and the kernel functions become

$$K_{\zeta-\beta} = \tfrac{1}{2}\gamma\beta\zeta(\beta^2 + \zeta^2 - 2\beta\zeta\cos\theta)^{-3/2} \quad (20)$$

$$K_{\eta-\beta} = \tfrac{1}{2}\gamma\eta(1-\beta)[\eta^2 + (1-\beta)^2 + 2\eta(1-\beta)\cos\theta]^{-3/2} \quad (21)$$

$$K_{\zeta-\eta} = \tfrac{1}{2}\gamma[(\eta-\zeta)^2 + 1 + 2(\eta-\zeta)\cos\theta]^{-3/2} \quad (22)$$

An investigation of the resulting equations reveals four independent dimensionless parameters that control the thermal behavior of an array: the blade opening angle, θ; the emissivity of the back surface, ϵ_1; the emissivity of the louver blades, ϵ_2; and the ratio of louver blade width to louver blade spacing, $b/L(b/L \geq 1.0)$. Their solution is discussed below.

Solutions

Because of the complexity of this set of simultaneous equations, solutions were obtained numerically using a digital computer. However, before numerical solutions could be undertaken, an investigation of the kernel functions [Eqs. (11–13) as transformed] revealed two problems: first, as the corners of the channel are approached (e.g., $\beta \to 0$ and $\zeta \to 0$ or $\beta \to 1$ and $\eta \to 0$), the first two kernel functions become indeterminate; and second, when $\theta = 0$, the first kernel function becomes indeterminate at $\beta = \zeta$.

The indeterminate situation at the corners occurs regardless of how the corners are approached (i.e., from the center of the back surface or downward along the blades). As a result, the kernel functions in all equations must be investigated. To handle the indeterminate situation for B^* with $\beta = 0$ and $\zeta = 0$, make the following substitution[3]: let $\tau = \beta/\zeta$ and

$$\begin{aligned} &\text{at} \quad \zeta = 0 \qquad \tau = \infty \\ &\text{at} \quad \zeta = b/L \qquad \tau = \beta(L/\beta) \end{aligned} \quad (23)$$

Substituting into the transformed Eq. (18) yields

$$B^* = \epsilon_1 + (1-\epsilon_1)\left[\int_{\beta(L/b)}^{\infty} C^*\left(\frac{\gamma}{2}\right)(\tau^2 + 1 - 2\tau\cos\theta)^{-3/2}\,d\tau + \int_0^{b/L} D^*K_{\eta-\beta}d\eta\right] \quad (24)$$

and as $\beta \to 0$,

$$B^*(0) = \epsilon_1 + (1-\epsilon_1) \times \left[\int_0^{\infty} C^*(0)\cdot\frac{\gamma}{2}(\tau^2 + 1 - 2\tau\cos\theta)^{-3/2}d\tau + \int_0^{b/L} D^*K_{\eta\text{-}0}d\eta\right] \quad (25)$$

$C^*(0)$ is a constant and, as such, can be pulled from the integral

$$B^*(0) = \epsilon_1 + (1-\epsilon_1) \times \left[\frac{1}{2}C^*(0)(1+\cos\theta) + \int_0^{b/L} D^*K_{\eta\text{-}0}\,d\eta\right] \quad (26)$$

By the same procedure, as $\beta \to 1$ and $\eta \to 0$, Eq. (27) becomes

$$B^*(1) = \epsilon_1 + (1-\epsilon_1)\left[\frac{1}{2}D^*(0) + \int_0^{b/L} C^*K_{\zeta\text{-}0}\,d\zeta\right] \quad (27)$$

As $\zeta \to 0$ and $\beta \to 1$ and $\eta \to 0$ and $\beta \to 1$, then

$$C^*(0) = \epsilon_2 T_2^*(0) + (1-\epsilon_2) \times \left[\frac{1}{2}B^*(0)(1+\cos\theta) + \int_0^{b/L} D^*K_{0\text{-}\eta}\,d\eta\right] \quad (28)$$

and

$$D^*(0) = \epsilon_2 T_3^*(0) + (1-\epsilon_2) \times \left[\frac{1}{2}B^*(1)(1-\cos\theta) + \int_0^{b/L} C^*K_{0\text{-}\eta}\,d\eta\right] \quad (29)$$

Consider next the situation when the kernel given by Eq. (20) becomes indeterminate ($\theta = 0, \zeta = \beta$ for the case when $b/L = 1.0$). To handle this situation, take the limit as θ approaches zero:

$$B^* = \epsilon_1 + (1 - \epsilon_1) \lim_{\theta \to 0} \int_0^1 C^* K_{\zeta\text{-}\beta}\, d\zeta \tag{30}$$

$$C^* = \epsilon_2 T_2^*(\zeta) + (1 - \epsilon_2) \lim_{\theta \to 0} \int_0^1 B^* K_{\zeta\text{-}\beta}\, d\beta \tag{31}$$

In the foregoing equations the integrals over surface 3 drop out. When $\theta = 0$, the back surface and the blades become parallel planes; and, because of assumption 3, they become, in effect, infinite parallel planes. Thus, from physical reasoning, the view of surface 1 from surface 2 (or the converse) becomes independent of location on either surface. Also the view factor of surface 3 to space becomes unity and is independent of location on surface 3. Consequently, B* and C* must be constants and can be pulled from the integrals in Eqs. (30) and (31).

If the kernel function is first integrated and then the limit taken, it can be shown that

$$\lim_{\theta \to 0} \int_0^1 K_{\zeta\text{-}\beta}\, d\zeta = 1 \tag{32}$$

Thus, for the case when $b/L = 1.0$, the transfer equations become

$$B^* = \epsilon_1 + (1 + \epsilon_1) C^* \tag{33}$$

$$C^* = \epsilon_2 T_2^* + (1 - \epsilon_2) B^* \tag{34}$$

$$D^* = \epsilon_3 T_3^* \tag{35}$$

$$2T_2^* = C^* + D^* \tag{36}$$

$$T_2^* = T_3^* \tag{37}$$

$$q''^* = \epsilon_1 (1 - B^*)/(1 - \epsilon_1) \tag{38}$$

For the case when $b/L > 1.0$, the same procedure can be applied to the overlapped region, from $\zeta = 1$ to $\zeta = b/L$, and from $\eta = 0$ to $\eta = b/L - 1.0$, to determine the transfer relationships in the overlapped region of the blades.

To solve the general forms of the transfer equations numerically, the power method was employed; an initial estimate was made for B^*, C^*, and D^*, and the equations were integrated by Simpson's rule. The new values of B^*, C^*, and D^* were then used in the next iteration. The process continued until convergence was achieved, which was assumed to have occurred when $q''^*(\beta)$ no longer changed in the third place. The solutions were checked by equating the net radiant heat transfer from the back surface to the total radiosity that escapes directly to space from all surfaces:

$$\int_0^1 q''^*(\beta) d\beta = \int_0^1 B^* M_1 d\beta + \int_0^{b/L} (C^* M_2\, d\zeta + D^* M_3\, d\eta) \tag{39}$$

The M's represent the form factors between the elemental areas $d\beta$, $d\zeta$, and $d\eta$, on surfaces 1, 2, and 3 and the open end of the channel. Expressions for the M terms are

$$M_1 = \frac{1 + (b/L)\cos\theta - \beta}{2\left[\left(1 + \frac{b}{L}\cos\theta - \beta\right)^2 + \left(\frac{b}{L}\sin\theta\right)^2\right]^{1/2}} + \frac{\beta - (b/L)\cos\theta}{2\left[\left(\beta - \frac{b}{L}\cos\theta\right)^2 + \left(\frac{b}{L}\sin\theta\right)^2\right]^{1/2}} \tag{40}$$

$$M_2 = \frac{1}{2} - \frac{b/L - \zeta + \cos\theta}{2\left[\left(\frac{b}{L} - \zeta + \cos\theta\right)^2 + (\sin\theta)^2\right]^{1/2}} \tag{41}$$

$$M_3 = \frac{1}{2} - \frac{b/L - \eta - \cos\theta}{2\left[\left(\frac{b}{L} = \eta - \cos\theta^2\right)^2 + (\sin\theta)^2\right]^{1/2}} \tag{42}$$

Results and Discussion

The primary objective was to relate effective emissivity of an array to blade opening angle and to study the effect thereon of black-surface emissivity, blade emissivity, and the ratio of blade width to blade spacing. To this end, solutions were obtained using an IBM 7094, for θ from 0° to 90° in increments of 5° or 10° for two to four values of each of ϵ_1, ϵ_2, and b/L.

Figure 2 is a plot of ϵ_T vs θ angle for various values of ϵ_1, with ϵ_2 and b/L constant. A quick calculation based on these results shows that the open value of effective emissivity is nearly a linear function (within 1.0 to 1.5%) of the back-surface emissivity for the range considered. On the other hand, the closed value of ϵ_T is nearly independent of ϵ_1. Of particular importance is the slope of ϵ_T curve at small values of θ. Within the first 20° to 25°, ϵ_T changes by an order of magnitude (from 0.025 to 0.25) at the specified small value of ϵ_2. Thus, if the designer wants to rely on the closed value of ϵ_T to achieve a thermal design objective, he must take care to guarantee that the blades will close completely and that heat leaks at the ends of a finite array are sealed.

Figure 3 shows that large changes in ϵ_2 have negligible effect on the open value of effective emissivity. If the temperature distributions on all surfaces making the channel were averaged and if effective emissivity calculations of an imaginary surface at the channel opening were based on this average temperature, it would be found that the channel acts nearly as a black cavity in relation to the average temperature. When the blades are closed the percent change in effective emissivity has nearly a 1:1 correspondence with the percent change in blade emissivity.

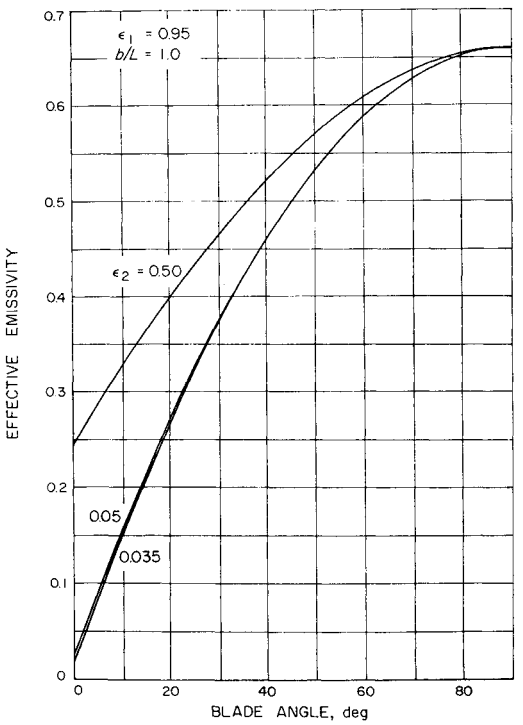

Fig. 3 Effective emissivity vs blade opening angle for various values of ϵ_2.

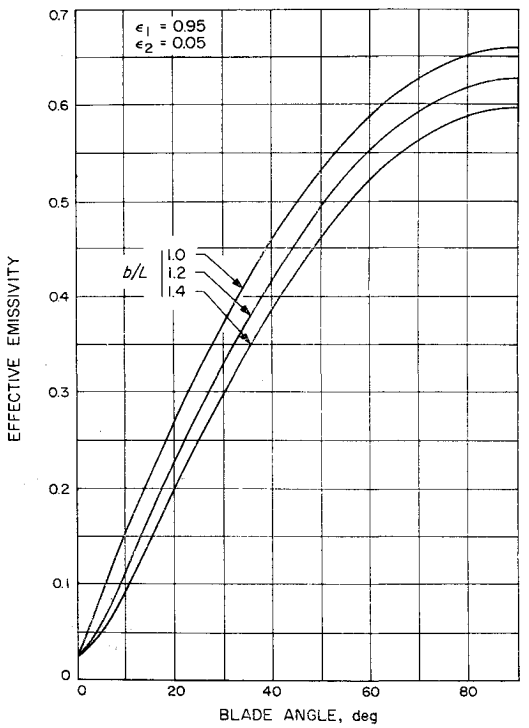

Fig. 4 Effective emissivity vs blade opening angle for various values of b/L.

Figure 4 shows the effect of increasing b/L on ϵ_T. From these curves the advantage of overlapping the blades can be seen in that, if the blades overlap, complete closure of the blades is not so critical; however, the open value of ϵ_T does suffer somewhat.

Figures 5 through 7 show the distribution of local heat transfer from the back surface, the radiosity distribution of the blades, and the temperature distribution in the blades, for the particular case of $\epsilon_1 = 0.95$, $\epsilon_2 = 0.05$, and $b/L = 1.0$. These plots indicate that it would be erroneous to assume that the radiosity distributions and the local heat-transfer rate are uniform. On the other hand, the rather large temperature gradients in the blades indicate, perhaps, that conduction in the blades should be taken into account, depending upon the material of the blades. If it is assumed that the blades are made of aluminum and their physical dimensions are of the order of 1.0 to 2.0 in. long and 0.0005 in. thick,[4] their efficiency as fins is quite good. This suggests that a uniform temperature for the blades would perhaps be

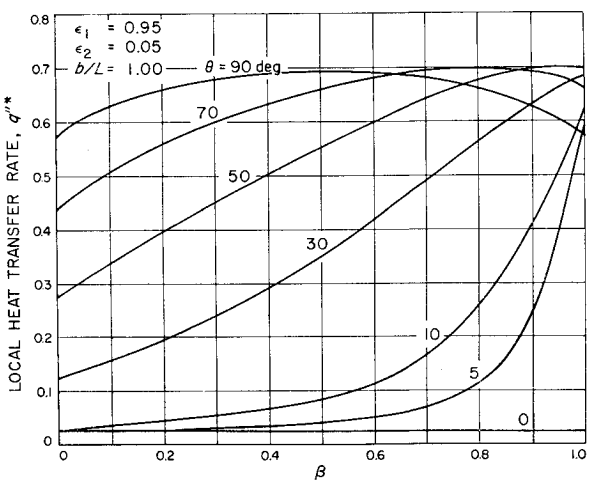

Fig. 5 Local heat-transfer rate from back surface at various blade angles.

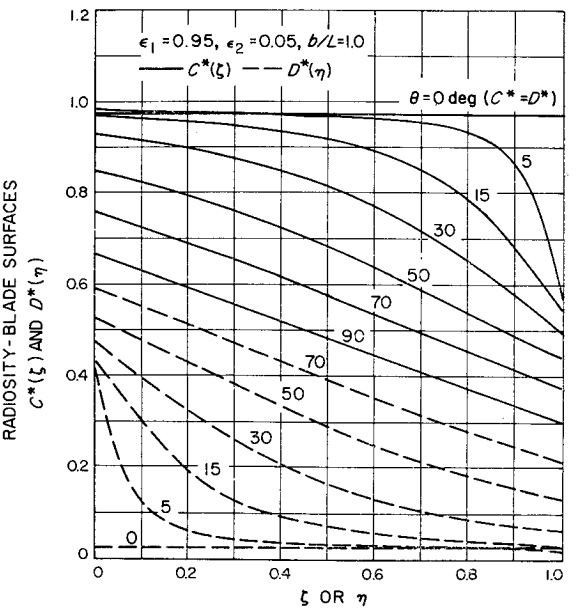

Fig. 6 Radiosity distributions along the blades at various blade angles.

a more reasonable assumption, however, to assume uniform temperature would add complexity to the transfer equations in that blade temperature is an unknown and, therefore, computations would have to be based on the average amount of irradiance absorbed by the blades, which would remain nonuniform. This would inject another integral into the equations. In the open position, conduction would tend to increase the value of ϵ_T, by transferring heat absorbed near the back surface to the tip where it could be more readily dissipated to space. If it is assumed that the blades are made from plastic, however, the resulting fin efficiency is quite low and the assumption made in this analysis is quite valid. In either case, the closed value of ϵ_T is negligibly affected by neglecting conduction, and the open value of ϵ_T predicted by the analysis is conservatively low. Consequently, the range of control as predicted by this analysis is less than it would actually be in operation.

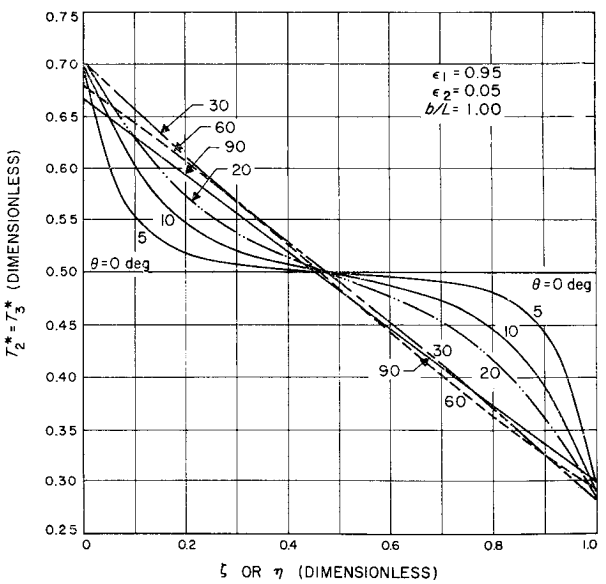

Fig. 7 Temperature distributions along the blades at various blade angles.

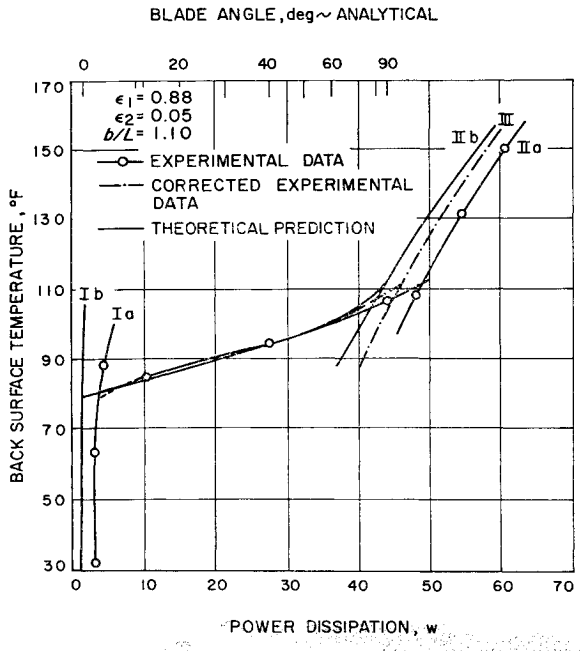

Fig. 8 Comparison of experimental and theoretical louver array performance.

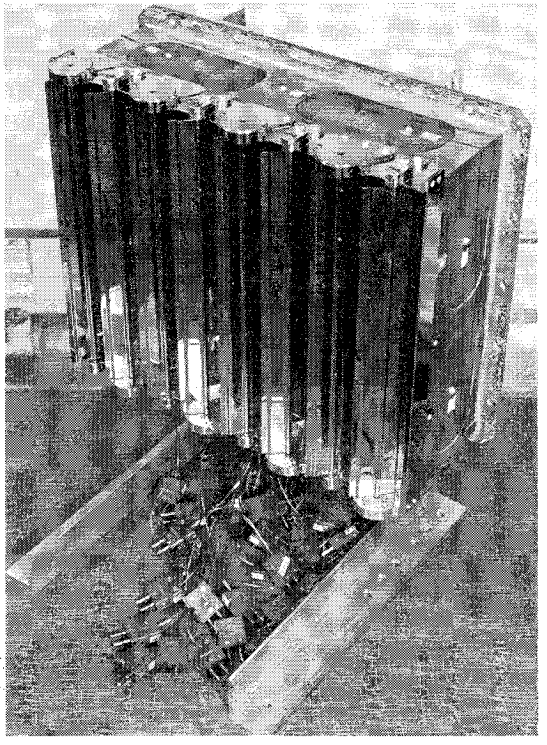

Fig. 9 Experimental test setup of the Mariner II louver system.

Comparison with Mariner II Data

Figure 8 is a photograph of the Mariner II louver array, including the bay to which it was mounted, and Fig. 9 is a comparison of its performance with the predicted performance. The louver array covered an area of 1.28 ft^2 and was designed to open over the temperature range from 80° to 112°F. The actuation mechanisms were bimetallic springs having approximately a linear response to temperature; that is, θ was approximately linear with temperature. Figure 9 gives T_1 as a function of the dissipated power. It should be emphasized that for the test data the dissipated power is from the entire louver system, which includes all external hardware making the system; hence, the experimental curves would be expected to fall somewhat to the right of the predicted curves. Curves labeled Ia and Ib are for the closed position, and IIa and IIb are for the open position; the curves between show the operation of the louvers as they open or close.

The discrepancy between curves Ia and Ib can be largely attributed to the dissipation from external hardware, but it can also be attributed, in part, to the finite size of the array and the consequent heat losses at the ends of the array. The discrepancy between curves IIa and IIb can be attributed to the same factors plus an additional consideration; namely, the blades in the test array are specular in their reflective characteristics, whereas the analysis assumed the blades to be diffuse. Curve III represents curve IIa corrected for heat dissipation from associated hardware and end effects (assuming these losses to be proportional to T_1^4). The experimental curves would move to the left when the discrepancy is corrected. This correction reduces the discrepancy between curves III and IIb to about 4.5%, and a similar correction to curve Ia made it coincide with Ib which suggests that the effect of specularity is about 4.5%. Thus, to assume that the blades are diffuse and, therefore, to utilize the resulting mathematical simplifications seems to have been a satisfactory procedure.

References

[1] Sparrow, E. M., Cregg, J. L., Szel, J. V., and Manos, P., "Analysis, results, and interpretation for radiation between some simply arranged gray surfaces," Trans. Am. Soc. Mech. Engrs., Ser. C, J. Heat Transfer **83,** 207–214 (1961).

[2] Jakob, M., *Heat Transfer* (John Wiley and Sons, Inc., New York, 1957), Vol. 2, Chap. 31.

[3] Heaslet, M. A. and Lomax, H., *Numerical Predictions of Radiative Interchange Between Conducting Fins with Mutual Irradiations* (NASA, Washington, D. C., 1961).

[4] Plamondon, J. A., "Thermal efficiency of coated fins," Trans. Am. Soc. Mech. Engrs., Ser. C, J. Heat Transfer **84,** 279–284 (1962).